



## Iron oxide nanoparticle preparation and its use for the removal of fluoride from aqueous solution: application of isotherm, kinetic, and thermodynamics

Abbas Rahdar<sup>a</sup>, Shahin Ahmadi<sup>b</sup>, Jie Fu<sup>c,\*</sup>, Somayeh Rahdar<sup>b,\*</sup>

<sup>a</sup> Department of Physics, University of Zabol, Zabol, P.O. Box. 35856-98613, Islamic Republic of Iran; email: a.rahdarnanophysics@gmail.com

<sup>b</sup> Department of Environmental Health, Zabol University of Medical Sciences, Zabol, Iran; emails: sh.ahmadi398@gmail.com (S. Ahmadi), rahdar89@gmail.com (S. Rahdar)

<sup>c</sup> Department of Environmental Science & Engineering, Fudan University, Shanghai 200438, China; email: jiefu@fudan.edu.cn

Received 14 May 2018; Accepted 24 October 2018

### ABSTRACT

Fluoride in drinking water above permissible levels is responsible for human and skeletal fluorosis. In this study, iron oxide nanoparticles ( $\text{Fe}_3\text{O}_4$ -NPs) were synthesized through an electrochemical method and used as an adsorbent for fluoride removal from aqueous solutions. The adsorption results indicated that  $\text{Fe}_3\text{O}_4$ -NPs could quickly capture fluoride in the initial 20 min, and the kinetic data could be well described by the pseudo-second-order model with a rate constant  $k_2$  of 0.100–0.187 g/mg.min. The adsorption isotherm data fitted better to the Langmuir model ( $R^2 = 0.969$ ) relative to Freundlich ( $R^2 = 0.851$ ), Temkin ( $R^2 = 0.743$ ), and Dubinin–Radushkevich ( $R^2 = 0.904$ ) models, indicating that monolayer adsorption occurred on the  $\text{Fe}_3\text{O}_4$ -NPs, and there was no interaction between adsorbed fluoride. Based on thermodynamics, the negative enthalpy ( $\Delta H^\circ = -0.011$  kJ/mol) indicated that the adsorption process was exothermic, and the negative entropy ( $\Delta S^\circ = -0.5$  kJ/mol.K) suggested that the degree of freedom at solid solution level declined during the adsorption process. In addition, the influences of important parameters including pH, adsorbent dosage, initial fluoride concentration, contact time, and temperature were investigated, and the optimal adsorption conditions were determined as pH 6,  $\text{Fe}_3\text{O}_4$ -NPs 0.02 g/L, initial fluoride 25 mg/L, contact time 45 min, and temperature 25°C.

**Keywords:** Fluoride; Nanoadsorbent; Adsorption; Kinetics; Thermodynamic; Isotherm

### 1. Introduction

The mineral constituents present in natural waters or contaminated source waters are found to become a potential risk for public health. Fluoride is a problematic inorganic ion, and the presence of excess fluoride in drinking water leads to serious health issues [1–3]. At low concentrations, it is essential for bone and teeth health, while at high concentrations, it leads to many health complications such as dental and skeletal fluorosis [4]. These complications are more serious in tropical regions where people consume large amounts of water, and the fluoride concentration increases in response to

strong evaporation [5]. In more extreme cases, it causes alteration of DNA structure, paralysis, and even death at ultra-high concentration [6]. Over 20 developed and developing countries have regions with endemic fluorosis, including Argentina, USA, Morocco, Libya, Algeria, Japan, Iraq, Egypt, Jordan, Kenya, Sri Lanka, China, Saudi Arabia, Thailand, India, Turkey, Syria, South Africa, Tanzania, and Iran [7]. According to the World Health Organization (WHO), the maximum acceptable concentration of fluoride in drinking water is 1.5 mg/L [8].

Considering the adverse health effects resulting from high fluoride concentration, suitable methods should be adopted to remove fluoride from water. There are various methods for

\* Corresponding authors.

the defluoridation of water including coagulation, membrane process, electrochemical treatment, ion exchange, and adsorption [9–11]. Many of these methods, such as electrochemical techniques and membrane processes, cannot be used on a large scale due to high costs of operation, repair and maintenance, high electricity consumption, production of toxic by-products, and complex operation. In contrast, adsorption process that is controlled by main physicochemical interactions, such as Van der Waals forces, hydrogen bonds, polarity, dipole–dipole interaction, and  $\pi$ – $\pi$  interaction, is one of the most cost-effective methods for water treatment [12–14]. It exploits the ability of certain solids to preferentially concentrate specific substance from solution onto their surfaces [15]. Especially, the development of various nano-adsorbents, which offer unique advantages including large specific surface area, selective and abundant adsorption sites, short intraparticle diffusion distance, tunable pore size, and easy regeneration and reusability, has attracted a great deal of attentions [16–18].

Iron oxide nanoparticles ( $\text{Fe}_3\text{O}_4$ -NPs) are known to be a promising nano-adsorbent for removing contaminants from aqueous environments, owing to their rich sources of raw materials, relatively easy synthesis, inexpensiveness, rapid reaction, high adsorption potency, and low toxicity [19–22].  $\text{Fe}_3\text{O}_4$  is an important member of spinel-type ferrite family, with a cubic inverse spinal structure of space group  $\text{Fd}\bar{3}m$  and an edge length of 0.839 nm [23]. Unfortunately, few studies have investigated the removal of fluoride from water by adsorption onto  $\text{Fe}_3\text{O}_4$ -NPs. In addition, most previous studies synthesized  $\text{Fe}_3\text{O}_4$ -NPs by co-precipitation method and used various surfactants to improve the surface area and to prevent the aggregation of nanoparticles [24]. However, the introduction of surfactants in the synthesis of  $\text{Fe}_3\text{O}_4$ -NPs may cause secondary pollution due to the potential toxicity of surfactants to aquatic organisms with the practical use of  $\text{Fe}_3\text{O}_4$ -NPs adsorbent in water treatment [25]. Therefore, green synthesis methods are needed to reduce the potential safety risks of  $\text{Fe}_3\text{O}_4$ -NPs adsorbent.

In this study,  $\text{Fe}_3\text{O}_4$ -NPs were synthesized through a surfactant-free electrochemical method and characterized by field emission scanning electron microscopy (FESEM), X-ray diffraction (XRD), vibration sample magnetization (VSM), and dynamic light scattering (DLS) techniques. The adsorption of fluoride from aqueous solution by as-prepared  $\text{Fe}_3\text{O}_4$ -NPs was comprehensively studied including adsorption kinetics, equilibrium isotherm, and thermodynamics. Also the influences of important parameters on the adsorption process including pH, adsorbent dosage, initial fluoride concentration, contact time, and temperature were systematically investigated.

## 2. Materials and methods

### 2.1. Preparation of $\text{Fe}_3\text{O}_4$ -NPs

Iron(II) sulfate heptahydrate ( $\text{FeSO}_4 \cdot 7\text{H}_2\text{O}$ , Sigma-Aldrich, Germany) and sodium hydroxide (NaOH, Sigma-Aldrich, Germany) were of analytical grade and were used as received without further purification.  $\text{Fe}_3\text{O}_4$ -NPs were synthesized using previously reported green surfactant-free electrochemical method [26], but here under vacuum system instead of the closed distilled water system. The reaction solution was NaOH aqueous solution with a pH value of 12.5.

### 2.2. Characterization of $\text{Fe}_3\text{O}_4$ -NPs

FESEM was performed using a Mira 3-XMU instrument with 700,000  $\times$  magnification (TESCAN, Brno–Czech Republic). XRD analysis was carried out using a D8 Advance X'Pert X-ray diffractometer with Cu  $K\alpha$  radiation (Bruker, Billerica, MA, USA). VSM was conducted using a Kavir precise magnetic instrument (Meghnatis Daghigh Kavir Company, Iran). DLS was measured using a Zetasizer Nano ZS instrument equipped with a He–Ne laser source (633 nm) with vertically polarized light (Malvern Instruments, UK).

### 2.3. Fluoride adsorption experiments

Different concentrations of fluoride solution were prepared from the stock solution of sodium fluoride (NaF, 500 mg/L); 100 mL of the fluoride solution was poured into an Erlenmeyer flask using a volumetric flask. If required, the solution pH was adjusted with 1 M HCl and NaOH solutions. Thereafter, certain amounts of  $\text{Fe}_3\text{O}_4$ -NPs were added into the Erlenmeyer flask, and the mixture was then immediately shaken on a shaker at a speed of 180 rpm. The samples were taken at set time intervals and filtered using Whatman filter paper (0.45  $\mu\text{m}$ ). The fluoride concentration of the samples was measured based on 4500-FD standard method using a spectrophotometer (CE-1021, Shimadzu, Tokyo, Japan) at the absorbance wavelength of 570 nm [27]. Studies indicate parameters such as adsorbate concentration, adsorbent dose, contact time, pH of the solution, and temperature that are crucial for optimizing the use of adsorbents in water treatment [15]. Thus, in this study, the important operating parameters were gradually changed to evaluate their effects on the adsorption process, including pH (3, 5, 6, 7, 8, and 9), adsorbent dosage (0.02, 0.05, 0.06, 0.07, and 0.09 g/L), initial fluoride concentration (5, 10, 15, 20, and 25 mg/L), contact time (20, 40, 60, 80, 100, and 120 min), and temperature (25°C, 35°C, and 45°C). Each experiment was replicated twice, and the mean values were reported. The adsorption capacity of fluoride onto  $\text{Fe}_3\text{O}_4$ -NPs ( $q_e$ , mg/g) and the removal efficiency ( $R$ , %) at equilibrium were calculated by the following equations [28]:

$$q_e = \frac{(C_0 - C_e)V}{M} \quad (1)$$

$$R = \frac{(C_0 - C_e)}{C_0} \times 100\% \quad (2)$$

where  $C_0$  (mg/L) and  $C_e$  (mg/L) are the initial and equilibrium concentration of fluoride in aqueous phase, respectively,  $V$  (L) is the volume of the solution, and  $M$  (g) is the mass of  $\text{Fe}_3\text{O}_4$ -NPs.

## 3. Results and discussion

### 3.1. Characterization of $\text{Fe}_3\text{O}_4$ -NPs

Fig. 1 presents the FESEM image of  $\text{Fe}_3\text{O}_4$ -NPs, and the obtained nanoparticles showed a relatively uniform size with an estimated mean value of 21 nm. Fig. 2 shows the XRD

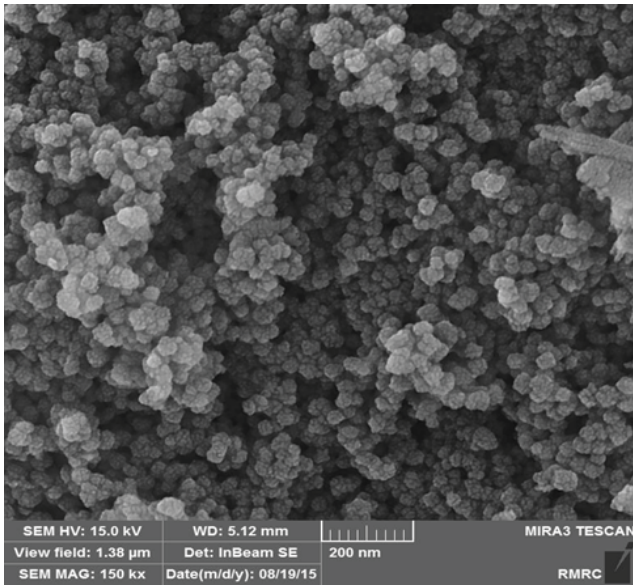


Fig. 1. FESEM image of  $\text{Fe}_3\text{O}_4$ -NPs.

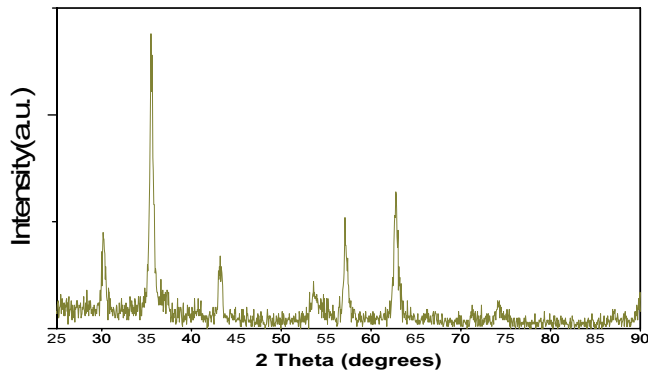


Fig. 2. XRD pattern of  $\text{Fe}_3\text{O}_4$ -NPs.

spectrum of  $\text{Fe}_3\text{O}_4$ -NPs. The Bragg peaks at  $2\theta$  of  $30.5^\circ$  (220),  $35.9^\circ$  (311),  $43.5^\circ$  (400),  $53.5^\circ$  (422),  $57.3^\circ$  (511),  $63.1^\circ$  (440), and  $74.1^\circ$  (533) are the expected signals from  $\text{Fe}_3\text{O}_4$ -NPs [29]. The average crystallite size ( $D$ ) of  $\text{Fe}_3\text{O}_4$ -NPs was calculated by the Scherer formula [30]:

$$D = \frac{K\lambda}{\beta \cos\theta} \quad (3)$$

where  $K$  is the dimensionless shape factor and has a typical value of about 0.9,  $\lambda$  is the wavelength of  $\text{Cu K}\alpha$  (1.542 Å),  $\beta$  is the full width at half maximum (FWHM) of the line, and  $\theta$  is the diffraction angle using (311) plane reflection from the XRD pattern. The calculated crystallite size of  $\text{Fe}_3\text{O}_4$ -NPs is 22 nm, which agrees with the FESEM observation.  $\text{Fe}_3\text{O}_4$ -NPs were further characterized by VSM (Fig. 3). Results indicated that the magnetic saturation of  $\text{Fe}_3\text{O}_4$ -NPs was considerably lower than that of bulk  $\text{Fe}_3\text{O}_4$  ( $\approx 92$  emu/g) [31], as is expected for the nanoformulation. From the VSM curve, it was also observed that the coercivity of  $\text{Fe}_3\text{O}_4$ -NPs was in agreement with the expected value for magnetite nanoparticles as reported in literature [29,31].

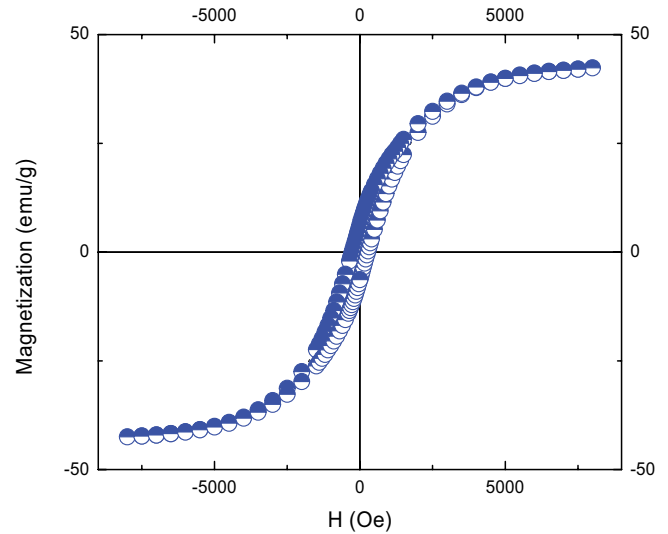


Fig. 3. Magnetization curve of  $\text{Fe}_3\text{O}_4$ -NPs.

DLS is a useful and effective tool to obtain the hydrodynamic size of nanometer-sized particles based on their Brownian motion within a dispersion solution. To characterize nanoparticles by the DLS technique, the normalized intensity–intensity autocorrelation function of the scattered light from nanometer-sized particles as a function of time,  $g^2(q, \tau)$ , for a given delay time  $\tau$  is given by the following equation [32–34]:

$$g^2(q, \tau) = \frac{\langle I(q, t)I(q, t + \tau) \rangle}{\langle I^2(q, t) \rangle} \quad (4)$$

where  $q$  is a particular wave vector,  $\tau$  is the delay time,  $I$  is the scattered light intensity, and the angular brackets  $\langle \rangle$  denote the expected value operator. The normalized autocorrelation function can be converted to the autocorrelation function of the scattered light electric field by the Siegert relationship [32–34]:

$$g^2(q, \tau) = 1 + |C \exp(-\Gamma\tau)|^2 \quad (5)$$

where  $C$  is the instrumental constant and  $\Gamma$  is the decay rate. For a solution containing mono-disperse particles, the first-order function  $g^1(q, \tau)$  is represented by a single exponential decay curve [32–34]:

$$g^1(q, \tau) = C \exp(-\Gamma\tau) \quad (6)$$

The decay rate  $\Gamma$  can be converted to the diffusion coefficient using Eq. (7) [32–34]:

$$D = \frac{\Gamma}{q^2} \quad (7)$$

Finally, the hydrodynamic radius of particles ( $R_h$ ) can be calculated using the Stokes–Einstein relation [32–34]:

$$R_h = \frac{K_B T}{6\eta\pi D} \quad (8)$$

where  $K_B$  is the Boltzmann's constant,  $T$  is the temperature (K), and  $\eta$  is the viscosity of continuous phase.

With DLS measurement, the change in hydrodynamic size of  $Fe_3O_4$ -NPs before and after adsorption was investigated. Fig. 4 shows the plot of the autocorrelation function of  $Fe_3O_4$ -NPs before and after adsorption by the DLS as a function of relaxation time. After calculation, the hydrodynamic size of  $Fe_3O_4$ -NPs before and after adsorption was 24.9 and 29.9 nm, respectively. Therefore, the aggregation of  $Fe_3O_4$ -NPs during the adsorption process was very weak, and  $Fe_3O_4$ -NPs adsorbent may be reused for many cycles after proper regeneration.

### 3.2. Adsorption kinetics

Adsorption of fluoride onto  $Fe_3O_4$ -NPs over time is displayed in Fig. 5. It is observed that  $Fe_3O_4$ -NPs could quickly capture fluoride from aqueous solution. The adsorption mainly occurred in the first 20 min and could rapidly reach equilibrium within 45 min for a varying initial fluoride concentration from 5 to 25 mg/L. The equilibrium adsorption capacity ranged from 23.25 to 123.35 mg/g.

Several kinetics models to examine the controlling mechanisms of adsorption process, such as chemical reaction, diffusion control, and mass transfer, are described in literatures [35,36]. Five kinetics models, namely pseudo-first-order, pseudo-second-order, intraparticle diffusion, Elovich model, and Bangham model, were used in this study to investigate the adsorption of fluoride on  $Fe_3O_4$ -NPs, and they can be expressed as [35,36]:

$$\text{Pseudo-first-order model: } \ln(q_e - q_t) = \ln q_e - k_1 t \quad (9)$$

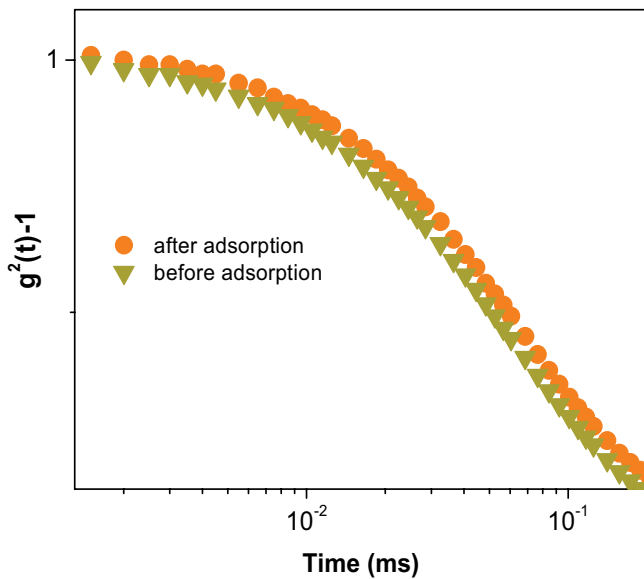


Fig. 4. The autocorrelation function of  $Fe_3O_4$ -NPs before and after adsorption versus relaxation time. Adsorption conditions: pH 6,  $Fe_3O_4$ -NPs 0.02 g/L, initial fluoride 25 mg/L, contact time 45 min, and temperature 25°C.

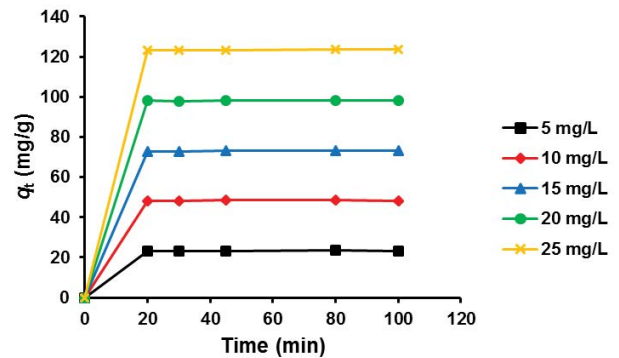


Fig. 5. Adsorption kinetics of fluoride onto  $Fe_3O_4$ -NPs. Experimental conditions: pH 6,  $Fe_3O_4$ -NPs 0.02 g/L, initial fluoride 25 mg/L, and temperature 25°C.

$$\text{Pseudo-second-order model: } \frac{t}{q_t} = \frac{1}{k_2 q_e^2} + \frac{t}{q_e} \quad (10)$$

$$\text{Intraparticle diffusion model: } q_t = k_p t^{0.5} + C \quad (11)$$

$$\text{Elovich model: } q_t = \frac{1}{\beta} \ln(\alpha\beta) + \frac{1}{\beta} \ln t \quad (12)$$

$$\text{Bangham model: } q_t = k_r t^{1/m} \quad (13)$$

where  $q_t$  (mg/g) and  $q_e$  (mg/g) are the adsorption capacities of fluoride at time  $t$  (min) and equilibrium, respectively.  $k_1$  ( $\text{min}^{-1}$ ),  $k_2$  ( $\text{g/mg}\cdot\text{min}$ ),  $k_p$  ( $\text{mg/g}\cdot\text{min}^{0.5}$ ), and  $k_r$  ( $\text{mg/g}\cdot\text{min}$ ) are the rate constants of the pseudo-first-order, pseudo-second-order, intraparticle diffusion, and Bangham models, respectively. For intraparticle diffusion model,  $C$  is the intercept (mg/g). If the intraparticle diffusion is involved in the adsorption process, then the plot of  $t^{0.5}$  versus  $q_t$  would result in a linear relationship, and the intraparticle diffusion would be the controlling step if this line passed through the origin ( $C = 0$ ). When the plots do not pass through the origin ( $C \neq 0$ ), this is indicative of some degree of boundary layer control, and this further shows that the intraparticle diffusion is not the only rate controlling step, but also other processes may control the rate of adsorption [37]. For Elovich model,  $\alpha$  ( $\text{g/mg}\cdot\text{min}$ ) is the initial rate, and parameter  $\beta$  (g/mg) is related to the extent of surface coverage and activation energy for chemisorptions.

Parameters of the five models are listed in Table 1. The goodness of fit of the models was expressed by the coefficients of determination ( $R^2$ ), and a relatively high  $R^2$  value indicated that the model successfully described the kinetics of fluoride sorption by  $Fe_3O_4$ -NPs. It was observed that, at low initial fluoride concentrations (5–20 mg/L), the sorption data were well represented by the pseudo-first-order model with the  $R^2$  values in the range of 0.997–1. However, when at the high initial fluoride concentration of 25 mg/L, no linear relationship was observed between  $\ln(q_e - q_t)$  and  $t$  ( $R^2 = 0$ ). Therefore, it was not appropriate to use the pseudo-first-order model to

Table 1  
Parameters of kinetics models for adsorption of fluoride onto  $\text{Fe}_3\text{O}_4$ -NPs. (Experimental conditions: pH 6,  $\text{Fe}_3\text{O}_4$ -NPs 0.02 g/L, initial fluoride 25 mg/L, and temperature 25°C.)

Kinetic parameters	Fluoride concentration (mg/L)				
	5	10	15	20	25
<b>Pseudo-first-order</b>					
$q_e$ (mg/g)	23.26	48.31	73.08	98.06	– <sup>a</sup>
$k_1$ (min <sup>-1</sup> )	0.215	0.328	0.267	0.355	–
$R^2$	0.9997	0.9999	0.9999	1	0
<b>Pseudo-second-order</b>					
$k_2$ (g/mg.min)	0.135	0.100	0.187	0.115	0.109
$q_e$ (mg/g)	21.18	48.07	72.99	98.03	123.45
$R^2$	0.9999	0.9999	1	1	1
<b>Intraparticle diffusion</b>					
$k_p$ (mg/g.min <sup>-0.5</sup> )	0.0711	–	0.0611	0.0478	0.0528
C	22.694	48.422	72.544	97.71	122.99
$R^2$	0.6212	0.0358	0.3747	0.2807	0.9504
<b>Elovich</b>					
$\alpha$ (g/mg.min)	–	–	–	–	–
$\beta$ (g/mg)	3.916	–	4.009	6.093	5.500
$R^2$	0.6649	0.013	0.4428	0.2247	0.9364
<b>Bangham</b>					
$k_r$ (mg/g.min)	22.241	–	72.064	97.421	122.674
$m$	91.74	–	293.25	598.80	680.27
$R^2$	0.5521	0	0.2564	0.0333	0.9153

<sup>a</sup> Cannot be calculated or gain the abnormal values.

predict the sorption kinetics of fluoride onto  $\text{Fe}_3\text{O}_4$ -NPs for the entire fluoride concentration range.

Adsorption is a multistep process involving transport of the solute molecules from the aqueous phase to the surface of the solid particles followed by diffusion of the solute molecules into the pore interiors. In a batch system with rapid stirring, there is a possibility that the transport of adsorbate from solution into the pores of the adsorbent is the rate controlling step. This possibility was tested in terms of intraparticle diffusion model [38]. The results showed that the intraparticle diffusion model could not fit well with the kinetic data due to the lower  $R^2$  values (0.0358–0.9504) and larger C values (22.694–122.99) (Table 1), suggesting that the intraparticle diffusion was not the rate controlling step for the sorption of fluoride onto  $\text{Fe}_3\text{O}_4$ -NPs.

The Elovich model is useful to describe the chemisorption kinetics, which are often interpreted as a combination of two or three simultaneous first-order reactions [39]. No linear relationship was found between  $q_t$  and  $\text{Ln}t$  ( $R^2 = 0.013$ – $0.9364$ ) (Table 1). Thus, the Elovich model is not applicable for the adsorption of fluoride onto  $\text{Fe}_3\text{O}_4$ -NPs. Similarly, the experimental data did not show a good fit for the Bangham model ( $R^2 = 0$ – $0.9153$ ) (Table 1), which confirmed that the pore diffusion is not the only rate-controlling step [40].

Finally, pseudo-second-order model has the best fit for adsorption kinetics of various initial concentrations of

fluoride, indicating that the adsorption of fluoride onto  $\text{Fe}_3\text{O}_4$ -NPs was a chemical adsorption process. Fig. 6 shows the linear fitting lines of pseudo-second-order model. Other works also reported that the adsorption of fluoride onto ion-exchange fiber [41] and  $\text{KMnO}_4$ -modified activated carbon [42] followed the pseudo-second-order kinetic pattern.

### 3.3. Adsorption isotherm

An important physiochemical subject in terms of the evaluation of adsorption processes is the adsorption isotherm, which provides a relationship between the amount of fluoride adsorbed on the solid phase and the concentration of fluoride in the solution when both phases are in equilibrium [43]. To analyze the experimental data and describe equilibrium status in adsorption between solid and liquid phases, Langmuir, Freundlich, Temkin, and Dubinin-Radushkevich isotherm models were used to fit the isotherm data. These models provided comprehensive and complete view about mechanism, surface properties, and adsorbing condition [35,36].

For the Langmuir model, it is assumed that adsorbates attach to certain and similar sites on the adsorbent's surface and the adsorption process occurs on the monolayer. Further, all adsorption sites have the same continuity in relation to the adsorbate molecules and no transition process happens from the adsorbate on the adsorbent surface [44], which can be presented by the following equation [28]:

$$q_e = \frac{q_m K_L C_e}{1 + K_L C_e} \quad (14)$$

where  $q_e$  (mg/g) is the amount of fluoride adsorbed per specific amount of adsorbent,  $C_e$  is equilibrium concentration of the fluoride solution (mg/L),  $K_L$  (L/mg) is Langmuir constant, and  $q_m$  (mg/g) is the maximum amount of fluoride required to form a monolayer. The Langmuir equation can be rearranged to linear form for the convenience of plotting and determining  $K_L$  and  $q_m$  with drawing the curve  $1/q_e$  versus  $1/C_e$  [35,36]:

$$\frac{1}{q_e} = \frac{1}{q_m} + \frac{1}{q_m K_L} \frac{1}{C_e} \quad (15)$$

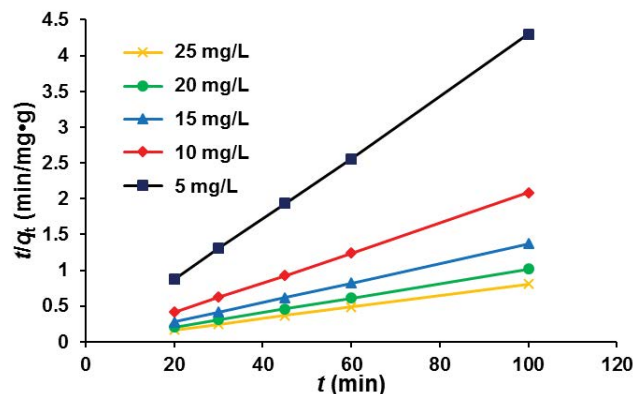


Fig. 6. Pseudo-second-order kinetic plots for adsorption of fluoride onto  $\text{Fe}_3\text{O}_4$ -NPs. Experimental conditions: pH 6,  $\text{Fe}_3\text{O}_4$ -NPs 0.02 g/L, initial fluoride 25 mg/L, and temperature 25°C.

The Freundlich model is an empirical relation between  $q_e$  and  $C_e$ . It is obtained by assuming a heterogeneous surface with nonuniform distribution of the adsorption sites on the adsorbent surface and can be expressed by the following equation [35,36]:

$$q_e = K_F C_e^{1/n} \tag{16}$$

where  $K_F$  and  $1/n$  are the Freundlich constants related to adsorption capacity and adsorption intensity, respectively. The Freundlich constants can be obtained by drawing the  $\text{Log}q_e$  versus  $\text{Log}C_e$  based on experimental data in light to linear equation [35,36]:

$$\text{Log}q_e = \text{Log}K_F + \frac{1}{n}\text{Log}C_e \tag{17}$$

In Temkin model, the surface absorption theory was corrected considering possible reactions between adsorbent-adsorbent and adsorbent-adsorbate. This model can be expressed as the following equation [43]:

$$q_e = B\text{Ln}K_T + B\text{Ln}C_e \tag{18}$$

where  $K_T$  and  $B$  are Temkin constants, and  $B$  is related to the heat of adsorption.

The empirical equation of Dubinin–Radushkevich model has been widely used to describe the adsorption of gases and vapors on microporous solids and can be written as [45]:

$$\text{Log}q_e = \text{Ln}q_m - \beta\varepsilon^2 \tag{19}$$

where  $\beta$  ( $\text{mol}^2/\text{KJ}^2$ ) is a constant connected with the mean free energy of adsorption per mole of the adsorbate,  $q_m$  ( $\text{mg/g}$ ) is the theoretical saturation capacity, and  $\varepsilon$  is the Polanyi potential.

The parameters of the four isotherm models are listed in Table 2. Examination of the Freundlich model fitting suggested that this model was not a perfect one for the experimental isotherm data ( $R^2 = 0.851$ ). The value of Freundlich exponent  $1/n = 0.197$  in the range 0.1–1 indicates the favorable adsorption [37]. The Temkin model assumes that heat

of adsorption (function of temperature) of all molecules in the layer would decrease linearly rather than logarithmic with coverage [46]. The Temkin fitting gained a  $R^2$  of 0.743, suggesting this model cannot well describe the sorption equilibrium of fluoride onto  $\text{Fe}_3\text{O}_4$ -NPs. The low  $B$  value (0.001) is an indication of non-physical adsorption process [46]. The Dubinin–Radushkevich isotherm is generally applied to express the adsorption mechanism with a Gaussian energy distribution onto a heterogeneous surface [47] and has often successfully fitted high solute activities and the intermediate range of concentrations data well. However, for the present isotherm data, this model did not show a good fit with a  $R^2$  of 0.904. Among the four isotherm models, the Langmuir model exhibited the best fit, according to the obtained  $R^2$  value of 0.969. This suggested that the Langmuir isotherm was adequate for modeling the adsorption of fluoride onto  $\text{Fe}_3\text{O}_4$ -NPs, which confirmed the monolayer coverage of fluoride onto  $\text{Fe}_3\text{O}_4$ -NPs and also the homogenous distribution of active sites on the material [37].

3.4. Effect of temperature and adsorption thermodynamics

The influence of temperature on fluoride adsorption was investigated by conducting experiment at different solution temperatures (298, 308, and 318 K). From Fig. 7, it can be seen that increase in solution temperature had an adverse effect on fluoride adsorption by  $\text{Fe}_3\text{O}_4$ -NPs. This performance may be attributed to the fact that a rise in temperature increases the tendency of fluoride ions to escape from the interface, thereby diminishing the amount of adsorption. Reduction in adsorption with increasing temperature indicates the exothermic nature of the adsorption process [45].

The thermodynamic parameters including the standard Gibbs free energy ( $\Delta G^\circ$ ), enthalpy change ( $\Delta H^\circ$ ), and entropy change ( $\Delta S^\circ$ ) can be evaluated by the following equations [35,36]:

$$K_c = \frac{q_e}{C_e} \tag{20}$$

$$\Delta G^\circ = -RT\text{Ln}K_c \tag{21}$$

Table 2  
Parameters of isotherm models for adsorption of fluoride onto  $\text{Fe}_3\text{O}_4$  nanoparticle. (Experimental conditions: pH 6,  $\text{Fe}_3\text{O}_4$ -NPs 0.02 g/L, and temperature 25°C.)

Langmuir		Temkin	
$q_m$ (mg/g)	19.44	$K_T$	— <sup>a</sup>
$K_L$ (L/mg)	2.372	$B$	0.001
$R^2$	0.969	$R^2$	0.743
Freundlich		Dubinin–Radushkevich	
$K_F$	20564.5	$q_m$ (mg/g)	4.830
$1/n$	0.197	$\beta$ ( $\text{mol}^2/\text{KJ}^2$ )	−707.2
$R^2$	0.851	$R^2$	0.904

<sup>a</sup> Gain the abnormal value.

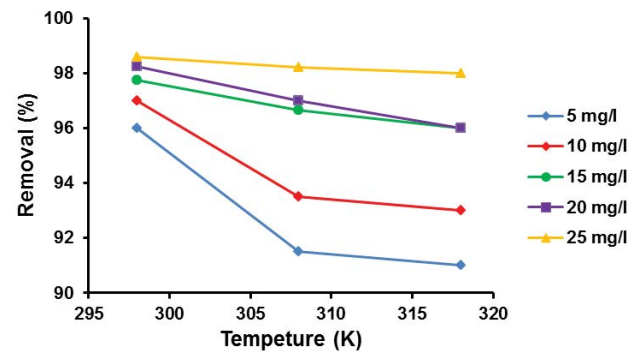


Fig. 7. Effects of temperature on adsorption of fluoride onto  $\text{Fe}_3\text{O}_4$ -NPs. Experimental condition: pH 6,  $\text{Fe}_3\text{O}_4$ -NPs dosage 0.02 g/L, and contact time 30 min.

$$\ln K_c = \frac{\Delta S^\circ}{R} - \frac{\Delta H^\circ}{RT} \quad (22)$$

where  $K_c$  is the equilibrium constant,  $q_e$  (mg/g) is the amount of adsorbed fluoride on  $\text{Fe}_3\text{O}_4$ -NPs at equilibrium, and  $C_e$  (mg/L) is the equilibrium concentration of the fluoride in the solution.  $R$  is the universal gas constant (8.314 J/mol.K), and  $T$  (K) is the temperature. The  $\Delta H^\circ$  and  $\Delta S^\circ$  values are derived from linear plot against  $1/T$ , which are from the slope and intercept, respectively.

The adsorption kinetics of fluoride onto  $\text{Fe}_3\text{O}_4$ -NPs were critically investigated at 298, 308, and 318 K, and the thermodynamic parameters were calculated as shown in Table 3. All the values of  $\Delta G^\circ$  were negative, and it showed that the adsorption process was spontaneous. The decrease of  $\Delta G^\circ$  happened with increase in temperature, indicating that the increasing temperature resulted in the increase of spontaneity. The negative  $\Delta H^\circ$  indicated that the adsorption process was exothermic. According to Le Chatelier's principle, increasing the temperature reduced the reaction rate, and it was followed by reducing the maximum adsorption capacity. The negative  $\Delta S^\circ$  showed that the degree of freedom at solid solution level declined during the adsorption process [48].

### 3.5. Effect of pH

The pH is an important parameter that influences on surface charges of adsorbents, ionization degree of different pollutants, and separation of functional groups on adsorbent active sites [49]. To obtain the optimal pH value, experiments were carried out by varying initial solution pH from 3 to 11, and under the condition of 20 mg/L of initial fluoride concentration, 0.1 g/L of  $\text{Fe}_3\text{O}_4$ -NPs dose, and 30 min of contact time. It can be seen from Fig. 8 that the adsorption of fluoride was highly dependent on the pH of the solution, and the maximum amount of removal of the fluoride ( $q_m = 19.75$  mg/g,  $R = 98.7\%$ ) was observed at pH 6. At relatively lower pH, positive ions predominated the adsorption sites, and the superficial charge of  $\text{Fe}_3\text{O}_4$ -NPs became more positive, which was beneficial for the enhanced attraction between fluoride anions and adsorbent surfaces [50]. On the other hand, with the continuous increase of pH, the adsorbent surface was deprotonated, and then the amount of  $\text{OH}^-$  ions increased on the nanoparticles' surface, which played a competing role for fluoride ions. In other words, with the adsorption of  $\text{OH}^-$  ions on  $\text{Fe}_3\text{O}_4$ -NPs surface, they occupied superficial sites, and then they made the superficial charge negative, causing increased repulsive force between fluoride anions

Table 3

Thermodynamic parameters for adsorption of fluoride onto  $\text{Fe}_3\text{O}_4$  nanoparticle. (Experimental conditions: pH 6,  $\text{Fe}_3\text{O}_4$ -NPs 0.02 g/L, initial fluoride 20 mg/L, and temperature 25°C.)

$T$ (K)	$\Delta G^\circ$ (kJ/mol)	$\Delta S^\circ$ (kJ/mol.K)	$\Delta H^\circ$ (kJ/mol)
298	-3.9437	-0.5	-0.011
308	-4.0630		
318	-4.1745		

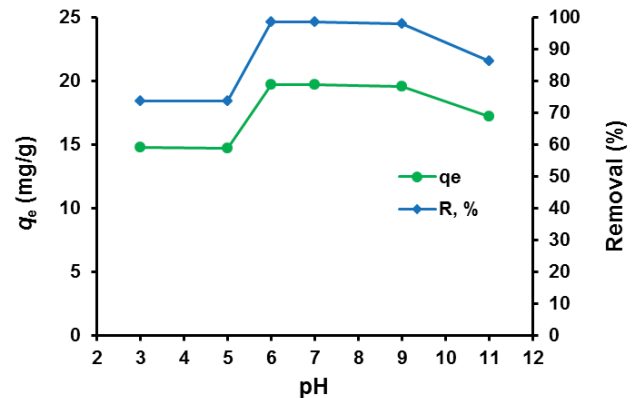


Fig. 8. Effect of pH on adsorption of fluoride onto  $\text{Fe}_3\text{O}_4$ -NPs. Experimental condition:  $\text{Fe}_3\text{O}_4$ -NPs dosage 0.1 g/L, initial fluoride 20 mg/L, temperature 25°C, and contact time 30 min.

and the adsorbent's surface, and thus decreasing the adsorption amount of fluoride [51]. Similar results were reported by Jagtap et al. [52] and Gloria et al. [53] that the removal of fluoride was maximum at a pH of 7 and 6.7, respectively.

### 3.6. Effect of $\text{Fe}_3\text{O}_4$ -NPs dosage

The adsorbent dosage is an important parameter to study the removal of fluoride from water by adsorption process, because this parameter determines the adsorption capacity of the adsorbent. To evaluate the effect of adsorbent dose on the adsorption of fluoride, 0.02 to 0.09 g/L of  $\text{Fe}_3\text{O}_4$ -NPs was used for adsorption experiments at the fixed conditions of pH 6, 20 mg/L of initial fluoride concentration, and 30 min of contact time. As it can be seen from Fig. 9, the removal efficiency of fluoride decreased slowly with increase in the adsorbent dosage from 0.02 to 0.09 g/L. A maximum removal of fluoride ( $q_m = 98.5$  mg/g,  $R = 98.5\%$ ) was achieved at an adsorbent concentration of 0.02 g/L. Therefore, the studied adsorbent  $\text{Fe}_3\text{O}_4$ -NPs has a high adsorption potential, and at very low dosage, it showed a very high adsorption capacity and removal efficiency. However, with the elevation of the adsorbent dosage, the fluoride removal was decreased, which may be due to accumulation of adsorbent particles and

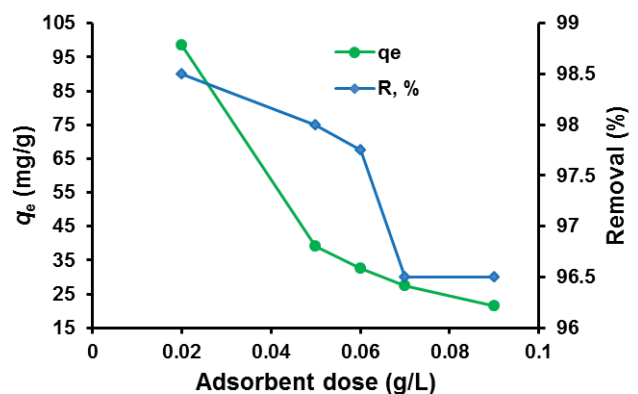


Fig. 9. Effect of adsorbent dosage on adsorption of fluoride onto  $\text{Fe}_3\text{O}_4$ -NPs. Experimental condition: pH 6, initial fluoride 20 mg/L, temperature 25°C, and contact time 30 min.

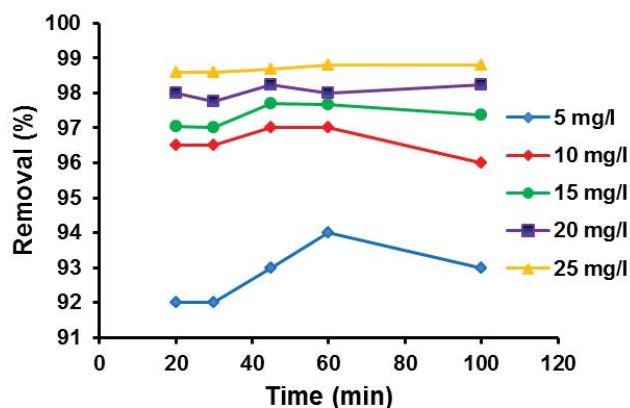


Fig. 10. Effects of contact time and initial fluoride concentration on adsorption of fluoride onto  $\text{Fe}_3\text{O}_4$ -NPs. Experimental condition: pH 6 and temperature  $25^\circ\text{C}$ .

development of electric repulsive force between adsorbent particles [53].

### 3.7. Effects of contact time and initial fluoride concentration

It is important to note that parameters such as the adsorbate concentration and contact time between adsorbent and adsorbate species play a significant role in the removal of pollutants from aqueous solutions. Therefore, the effect of contact time on the fluoride adsorption by  $\text{Fe}_3\text{O}_4$ -NPs was investigated for 120 min at different initial fluoride concentrations (Fig. 10). The fluoride was rapidly adsorbed in the first 45 min ( $R = 93$ – $98.68\%$ ) for various initial fluoride concentrations, and then, the removal efficiency showed a slight decrease from 45 to 120 min. Therefore, the removal of fluoride ions increased with increase in contact time to some extent, but further increase in the contact time did not increase the uptake due to deposition of fluoride ion on the vacant sites of adsorbent. Upon a fixed contact time, when the initial fluoride concentration was increased, the removal efficiency of fluoride also increased, which may be due to excessive accumulation of fluoride ions around the adsorbent and increased chance of collision.

## 4. Conclusions

The adsorption of fluoride onto  $\text{Fe}_3\text{O}_4$ -NPs was comprehensively investigated. For adsorption kinetics, the pseudo-second-order models can well describe the experimental data, indicating that the adsorption process was controlled by chemical interaction. For adsorption isotherms, the Langmuir model could fit the experimental data better than the other models, suggesting a monolayer adsorption process. The thermodynamics study showed that the adsorption process was spontaneous, exothermic, and irreversible. In addition, the effects of various operating parameters were investigated, and the optimum conditions were determined as follows: pH = 6,  $\text{Fe}_3\text{O}_4$ -NPs = 0.02 g/L, initial fluoride = 25 mg/L, contact time = 45 min, and temperature =  $25^\circ\text{C}$ . Due to the strong adsorption capacity and easy recovery through magnetism,  $\text{Fe}_3\text{O}_4$ -NPs is a promising nano-adsorbent in the treatment of fluoride-contaminated water.

## Acknowledgments

The authors would like to thank University of Zabol for financial supporting this work. Dr. Jie Fu thanks the financial support from the Power China Huadong Engineering Corporation (KY2016-02-04).

## Symbols

$\Delta G^\circ$	—	Gibbs free energy change
$\Delta H^\circ$	—	Enthalpy change
$\Delta S^\circ$	—	Entropy change
$C_0$	—	Initial concentration in aqueous phase
$C_e$	—	Equilibrium concentration in aqueous phase
$D$	—	Crystallite size
DLS	—	Dynamic light scattering
$\text{Fe}_3\text{O}_4$ -NPs	—	Iron oxide nanoparticles
FESEM	—	Field emission scanning electron microscopy
$k$	—	Rate constant
$K_F$	—	Freundlich constant
$K_L$	—	Langmuir constant
$K_T$	—	Temkin constant
$M$	—	Mass
$q_e$	—	Adsorption capacity at equilibrium
$q_m$	—	Maximum adsorption capacity
$q_t$	—	Adsorption capacity at time $t$
$R$	—	Universal gas constant
$R$ (%)	—	Removal efficiency
$T$	—	Temperature
VSM	—	Vibration sample magnetization
XRD	—	X-ray diffraction

## References

- [1] V.K. Gupta, I. Ali, Environmental Water: Advances in Treatment, Remediation and Recycling, Elsevier Inc., Amsterdam, Netherlands, 2012.
- [2] I. Ali, Instrumental Methods in Metal Ions Speciation: Chromatography, Capillary Electrophoresis and Electrochemistry, Taylor & Francis Ltd., New York, USA, 2006.
- [3] E. Bazrafshan, D. Balarak, A. Panahi, H. Kamani, A. Mahvi, Fluoride removal from aqueous solutions by cupric oxide nanoparticles, Fluoride, 49 (2016) 233–244.
- [4] S.S. Tripathy, J.L. Bersillon, K. Gopal, Removal of fluoride from drinking water by adsorption onto alum-impregnated activated alumina, Sep. Purif. Technol., 50 (2006) 310–317.
- [5] R. Yao, F. Meng, L. Zhang, D. Ma, M. Wang, Defluoridation of water using neodymium-modified chitosan, J. Hazard. Mater., 165 (2009) 454–460.
- [6] M. Hernández-Campos, A.M.S. Polo, M. Sánchez-Polo, J. Rivera-Utrilla, M.S. Berber-Mendoza, G. Andrade-Espinosa, M.V. López-Ramón, Lanthanum-doped silica xerogels for the removal of fluorides from waters, J. Environ. Manage., 213 (2018) 549–554.
- [7] Meenakshi, R.C. Maheshwari, Fluoride in drinking water and its removal, J. Hazard. Mater., 137 (2006) 456–463.
- [8] Y. Çengelöglu, E. Kir, M. Ersöz, Removal of fluoride from aqueous solution by using red mud, Sep. Purif. Technol., 28 (2002) 81–86.
- [9] M. Mohapatra, S. Anand, B.K. Mishra, D.E. Giles, P. Singh, Review of fluoride removal from drinking water, J. Environ. Manage., 91 (2009) 67–77.
- [10] M. Arora, R.C. Maheshwari, S.K. Jain, A. Gupta, Use of membrane technology for potable water production, Desalination, 170 (2004) 105–112.
- [11] D. Balarak, Y. Mahdavi, E. Bazrafshan, A.H. Mahvi, Y. Esfandyari, T. Sari, Adsorption of fluoride from aqueous solutions by

- carbon nanotubes: determination of equilibrium, kinetic, and thermodynamic parameters, *Fluoride*, 49 (2016) 71–83.
- [12] J. Fu, W.-N. Lee, C. Coleman, M. Meyer, J. Carter, K. Nowack, C.-H. Huang, Pilot investigation of two-stage biofiltration for removal of natural organic matter in drinking water treatment, *Chemosphere*, 166 (2017) 311–322.
- [13] A.A. Basheer, New generation nano-adsorbents for the removal of emerging contaminants in water, *J. Mol. Liq.*, 261 (2018) 583–593.
- [14] E. Bazrafshan, F.K. Mostafapour, S. Rahdar, A.H. Mahvi, Equilibrium and thermodynamics studies for decolorization of Reactive Black 5 (RB5) by adsorption onto MWCNTs, *Desal. Water Treat.*, 54 (2015) 2241–2251.
- [15] E. Bazrafshan, P. Amirian, A. Mahvi, A. Ansari-Moghaddam, Application of adsorption process for phenolic compounds removal from aqueous environments: A systematic review, *Global Nest J.*, 18 (2016) 146–163.
- [16] Z. Cai, A.D. Dwivedi, W.-N. Lee, X. Zhao, W. Liu, M. Sillanpaa, D. Zhao, C.-H. Huang, J. Fu, Application of nanotechnologies for removing pharmaceutically active compounds from water: development and future trends, *Environ. Sci. Nano*, 5 (2018) 27–47.
- [17] I. Ali, Z.A. Allothman, A. Alwarthan, Uptake of propranolol on ionic liquid iron nanocomposite adsorbent: Kinetic, thermodynamics and mechanism of adsorption, *J. Mol. Liq.*, 236 (2017) 205–213.
- [18] S.I. Siddiqui, R. Ravi, G. Rathi, N. Tara, S.U. Islam, S.A. Chaudhry, Decolorization of Textile Wastewater Using Composite Materials, S.U. Islam, B.S. Butola Eds., *Nanomaterials in the Wet Processing of Textiles*, John Wiley & Sons, Inc., New York, USA, 2018, pp. 187–218.
- [19] I. Ali, Z.A. Al-Othman, A. Al-Warthan, Removal of secbumeton herbicide from water on composite nanoadsorbent, *Desal. Water Treat.*, 57 (2016) 10409–10421.
- [20] I. Ali, Z.A. Allothman, M.M. Sanagi, Green Synthesis of Iron Nano-Impregnated Adsorbent for Fast Removal of Fluoride from Water, *J. Mol. Liq.*, 211 (2015) 457–465.
- [21] S.I. Siddiqui, S.A. Chaudhry, Iron oxide and its modified forms as an adsorbent for arsenic removal: A comprehensive recent advancement, *Process Saf. Environ. Prot.*, 111 (2017) 592–626.
- [22] S.I. Siddiqui, S.A. Chaudhry, Removal of arsenic from water through adsorption onto metal oxide-coated material, *Mater. Res. Found.*, 15 (2017) 227–276.
- [23] W.H. Bragg, The Structure of Magnetite and the Spinels, *Nature*, 95 (1915) 561–561.
- [24] S. Rajput, C.U. Pittman, D. Mohan, Magnetic magnetite (Fe<sub>3</sub>O<sub>4</sub>) nanoparticle synthesis and applications for lead (Pb<sup>2+</sup>) and chromium (Cr<sup>6+</sup>) removal from water, *J. Colloid Interface Sci.*, 468 (2016) 334–346.
- [25] S. Rebello, A.K. Asok, S. Mundayoor, M.S. Jisha, Surfactants: toxicity, remediation and green surfactants, *Environ. Chem. Lett.*, 12 (2014) 275–287.
- [26] F. Fajaroh, H. Setyawan, W. Widiyastuti, S. Winardi, Synthesis of magnetite nanoparticles by surfactant-free electrochemical method in an aqueous system, *Adv. Powder Technol.*, 23 (2012) 328–333.
- [27] EPA (Environmental Protection Agency USA), in, EPA, Washington DC, USA, 1993, pp. 1–2.
- [28] W. Liu, X. Zhao, T. Wang, J. Fu, J. Ni, Selective and irreversible adsorption of mercury(II) from aqueous solution by a flower-like titanate nanomaterial, *J. Mater. Chem. A*, 3 (2015) 17676–17684.
- [29] N. Nishida, S. Amagasa, Y. Kobayashi, Y. Yamada, Synthesis of superparamagnetic δ-FeOOH nanoparticles by a chemical method, *Appl. Surf. Sci.*, 387 (2016) 996–1001.
- [30] M. Aliahmad, A. Rahdar, F. Sadeghfar, S. Bagheri, M. Hajinezhad, Synthesis and Biochemical effects of magnetite nanoparticle by surfactant-free electrochemical method in an aqueous system: The current density effect, *Nanomed. Res. J.*, 1 (2016) 39–46.
- [31] S. Maryamdokht Taimoory, J.F. Trant, A. Rahdar, M. Aliahmad, F. Sadeghfar, M. Hashemzaei, Importance of the inter-electrode distance for the electrochemical synthesis of magnetite nanoparticles: Synthesis, characterization, computational modelling, and cytotoxicity, *e-J. Surf. Sci. Nanotechnol.*, 15 (2017) 31–39.
- [32] A. Rahdar, M. Almasi-Kashi, Photophysics of Rhodamine B in the nanosized water droplets: A concentration dependence study, *J. Mol. Liq.*, 220 (2016) 395–403.
- [33] A. Rahdar, M. Almasi-Kashi, N. Mohamed, Light scattering and optic studies of Rhodamine B-comprising cylindrical-like AOT reversed micelles, *J. Mol. Liq.*, 223 (2016) 1264–1269.
- [34] A. Rahdar, M. Almasi-Kashi, M. Aliahmad, Effect of chain length of oil on location of dye within AOT nanometer-sized droplet microemulsions at constant water content, *J. Mol. Liq.*, 233 (2017) 398–402.
- [35] J. Fu, R. Song, W.J. Mao, Q. Wang, S.Q. An, Q.F. Zeng, H.L. Zhu, Adsorption of disperse blue 2BLN by microwave activated red mud, *Environ. Prog. Sustain.*, 30 (2011) 558–566.
- [36] F. Peng, P.W. He, Y. Luo, X. Lu, Y. Liang, J. Fu, Adsorption of phosphate by biomass char deriving from fast pyrolysis of biomass waste, *Clean – Soil Air Water*, 40 (2012) 493–498.
- [37] G. Crini, H.N. Peindy, F. Gimbert, C. Robert, Removal of C.I. Basic Green 4 (Malachite Green) from aqueous solutions by adsorption using cyclodextrin-based adsorbent: Kinetic and equilibrium studies, *Sep. Purif. Technol.*, 53 (2007) 97–110.
- [38] W. Weber, J. Morris, Kinetics of adsorption on carbon from solution, *J. Sanit. Eng. Div. Am. Soc. Civ. Eng.*, 89 (1963) 31–60.
- [39] S.H. Chien, W.R. Clayton, Application of Elovich equation to the kinetics of phosphate release and sorption in soils, *Soil Sci. Soc. Am. J.*, 44 (1980) 265–268.
- [40] N.Y. Mezenner, A. Bensmaili, Kinetics and thermodynamic study of phosphate adsorption on iron hydroxide-eggshell waste, *Chem. Eng. J.*, 147 (2009) 87–96.
- [41] L. Ruixia, G. Jinlong, T. Hongxiao, Adsorption of fluoride, phosphate, and arsenate ions on a new type of ion exchange fiber, *J. Colloid Interface Sci.*, 248 (2002) 268–274.
- [42] A.A.M. Daifullah, S.M. Yakout, S.A. Elreefy, Adsorption of fluoride in aqueous solutions using KMnO<sub>4</sub>-modified activated carbon derived from steam pyrolysis of rice straw, *J. Hazard. Mater.*, 147 (2007) 633–643.
- [43] S.A. Chaudhry, Z. Zaidi, S.I. Siddiqui, Isotherm, kinetic and thermodynamics of arsenic adsorption onto Iron-Zirconium Binary Oxide-Coated Sand (IZBOCS): Modelling and process optimization, *J. Mol. Liq.*, 229 (2017) 230–240.
- [44] S.I. Siddiqui, G. Rathi, S.A. Chaudhry, Acid washed black cumin seed powder preparation for adsorption of methylene blue dye from aqueous solution: Thermodynamic, kinetic and isotherm studies, *J. Mol. Liq.*, 264 (2018) 275–284.
- [45] D. Mohapatra, D. Mishra, S.P. Mishra, G.R. Chaudhury, R.P. Das, Use of oxide minerals to abate fluoride from water, *J. Colloid Interface Sci.*, 275 (2004) 355–359.
- [46] M.I. Tempkin, V. Pyzhev, Kinetics of ammonia synthesis on promoted iron catalyst, *Acta Phys. Chim. USSR*, 12 (1940) 327–356.
- [47] A. Günay, E. Arslankaya, İ. Tosun, Lead removal from aqueous solution by natural and pretreated clinoptilolite: Adsorption equilibrium and kinetics, *J. Hazard. Mater.*, 146 (2007) 362–371.
- [48] P.M. Pimentel, M.A.F. Melo, D.M.A. Melo, A.L.C. Assunção, D.M. Henrique, C.N.S. Jr, G. González, Kinetics and thermodynamics of Cu(II) adsorption on oil shale wastes, *Fuel Process. Technol.*, 89 (2008) 62–67.
- [49] S. Moghaddam, S. Rahdar, M. Taghavi, Cadmium removal from aqueous solutions using saxaul tree ash, Iran. *J. Chem. Chem. Eng.*, 35 (2015) 45–52.
- [50] M. Mahramanlioglu, I. Kizilcikli, I.O. Bicer, Adsorption of fluoride from aqueous solution by acid treated spent bleaching earth, *J. Fluorine Chem.*, 115 (2002) 41–47.
- [51] K. Smitha, S.G. Thampi, Experimental investigations on fluoride removal from water using nanoalumina-carbon nanotubes blend, *J. Water Resource Prot.*, 9 (2017) 760–769.
- [52] S. Jagtap, D. Thakre, S. Wanjari, S. Kamble, N. Labhsetwar, S. Rayalu, New modified chitosan-based adsorbent for defluoridation of water, *J. Colloid Interface Sci.*, 332 (2009) 280–290.
- [53] S. Ghorai, K.K. Pant, Equilibrium, kinetics and breakthrough studies for adsorption of fluoride on activated alumina, *Sep. Purif. Technol.*, 42 (2005) 265–271.